

Ground-Based Determination of Low Altitude Temperature Profiles by Microwaves

ED R. WESTWATER—*Environmental Research Laboratories, NOAA, Boulder, Colo., and Department of Physics, University of Colorado, Boulder, Colo.*

ABSTRACT—Vertical temperature profiles of the lower atmosphere are determined from clear air ground-based measurements of microwave thermal emission by oxygen. Angular emission data from two diverse meteorological locations are mathematically inverted by statistical techniques to recover the vertical profiles. Inversion of 52.5 GHz data, gathered at Upolu Point, Hawaii, Hawaii, resulted in an average root-mean-square (rms) difference of 1.27°K between inverted and radiosonde measured profiles from 0 to 10 km. Pressure and humidity profiles are simultaneously estimated from the data; numerical integration of the inverted humidity profiles results in a determination of total vertical water content with a relative accuracy of about 10 percent. Radiometer emission data at 54.0, 54.5, and 55.0 GHz, taken at Salt Lake City, Utah, are inverted with resulting average rms differences of 1.17°K over the

height interval from 0 to 6.4 km. A priori temperature variance, corresponding to known surface conditions, is reduced by a factor of 8 to 1. Ground-based thermal inversions are successfully recovered. For both locations, the rms accuracies agree well with predictions based on the theory of statistical estimation.

The statistical inversion equations of Rodgers, and Strand and Westwater are extended for the purpose of inferring profiles from spectrally contaminated radiation measurements. The equations require auto- and cross-covariance matrices of all meteorological variables that contribute to the emission. The general linear estimation equations of Deutsch are applied to a linear approximation to the radiative transfer equation to derive the inversion equations. An analysis of the linearization errors is given.

1. INTRODUCTION

The remote sensing of low altitude vertical temperature profiles is of great interest in studies of air pollution. Previous theoretical results have indicated that passive ground-based microwave measurements of thermal emission by oxygen can provide significant information on the temperature structure up to about 2 or 3 km under clear atmospheric conditions (Westwater and Strand 1968, Mount et al. 1968).

Temperature profiles have been recovered from radiometric data by using a variety of mathematical techniques (Chahine 1970, Smith et al. 1970, Wark 1970). The technique presented here utilizes statistical characteristics of atmospheric variables contributing to the observed emission for the construction of a physically significant solution to the inverse problem of radiative transfer. This method retains features of the earlier statistical inversion techniques of Rodgers (1966) and Strand and Westwater (1968) but also permits the effect of background atmospheric noise (such as that from water vapor fluctuations) to be estimated.

The inversion equations are applied to single-frequency radiometer scan data, and the results are compared with concurrent radiosonde measurements. The data were taken at two diverse meteorological locations:

1. Upolu Point, Hawaii, Hawaii. Angular measurements at 52.5 GHz are used to derive temperature profiles with a root-mean-square (rms) error of 1.25°K over a 10-km height interval. The brightness spectrum is shown to be substantially affected by water vapor at the higher elevation angles. The integrated vertical water content was also determined from the radiometric data and compared

with water content derived from radiosonde measurements to about 10 percent.

2. Salt Lake City, Utah. Discrete angular data at 54.0, 54.5, and 55.0 GHz are used to derive temperature profiles with an rms accuracy of about 0.5°K up to 2 km. Both lapse and ground-based inversion profiles are encountered and successfully recovered.

2. INVERSION METHOD

The problem of remotely inferring temperature profiles from radiation measurements can be regarded as a problem in statistical estimation (Rodgers 1966, Strand and Westwater 1968). A related problem of filtering a signal from noise was solved by Foster (1961). If the contributions to brightness temperature fluctuations caused by temperature fluctuations are regarded as the desired signal, then all other contributions to this signal may be considered as noise. This noise may arise from instrumental noise or from effects of atmospheric origin, such as pressure, water vapor, or clouds. If the a priori statistical behavior of the signal and the noise is known, this knowledge can be used to construct a filter or an optimum estimator using the minimum expected mean square error criterion of Wiener (1949). The linear method for achieving the minimum variance estimator from past data will be presented below by extending the equations of Foster (1961), Rodgers (1966), and Strand and Westwater (1968) to those equations applicable when the contaminating noise is correlated with the desired signal. In addition, the effective noise level of background fluctuations is determined and the reduction of this noise using surface constraints is discussed.

Statistical inversion techniques attempt to derive atmospheric profiles by using radiation measurements to form statistical estimates. This is a specific example of a general problem in statistical estimation, that of estimating one vector quantity from measurements of another. The linear solution of this general problem is outlined below, following Deutsch (1965).

Consider two (column) vectors, \mathbf{x} and \mathbf{y} , the components of which are random variables. For our purposes, \mathbf{y} can be regarded as a vector representing an atmospheric profile and \mathbf{x} as a vector of measurements. If the dimensions of \mathbf{x} and \mathbf{y} are n and m , respectively, then the quantities are described by a $(n+m)$ -dimensional joint probability distribution. Let $E\{ \}$ be the expected value operator over this distribution. Denote the mean, or average, of any vector \mathbf{x} by $\langle \mathbf{x} \rangle \equiv E\{\mathbf{x}\}$ and the departure of \mathbf{x} from its mean by $\mathbf{x}' \equiv \mathbf{x} - \langle \mathbf{x} \rangle$. In the following, we will consistently use primes on statistical quantities to denote departures from average values. Deutsch shows that \mathbf{y}' may be estimated as a linear function of \mathbf{x}' by the minimum variance estimator, $\hat{\mathbf{y}}'$ where

$$\hat{\mathbf{y}}' = S_{\mathbf{y}\mathbf{x}} S_{\mathbf{x}}^{-1} \mathbf{x}', \quad (1)$$

$$S_{\mathbf{y}\mathbf{x}} \equiv E\{\mathbf{y}' \mathbf{x}'^*\}, \quad (2)$$

and

$$S_{\mathbf{x}} \equiv E\{\mathbf{x}' \mathbf{x}'^*\}. \quad (3)$$

The superscript * means matrix transposition, and the standard statistical notation of designating estimators by the superscript ^ has been followed. The i, j element of the $m \times n$ matrix $S_{\mathbf{y}\mathbf{x}}$ is the cross-covariance of y_i and x_j ; similarly, the i, j element of the $n \times n$ matrix $S_{\mathbf{x}}$ is the autocovariance of x_i and x_j . The determination of the above matrices, which are defined with respect to an ensemble average over an infinite population, usually requires averaging over a finite sample.

The equations outlined above may be applied to the inversion problem in several different ways depending on the data at one's disposal. The most direct application occurs by correlating a representative sample of simultaneous direct measurements of both the vertical temperature profile and either spectral or angular measurements of brightness. The coefficient matrix relating the vector representation of the temperature profile, \mathbf{T} , to the vector of measurements, \mathbf{T}_b , is determined simply by linear regression. This technique has been discussed recently by Smith et al. (1970).

When the absorption and emission characteristics are known as a function of meteorological parameters, the "pseudo-regression" coefficients, $S_{\mathbf{T}, \mathbf{T}_b} S_{\mathbf{T}_b}^{-1}$, may be approximated by calculations taken over a representative history of meteorological data. The noise levels associated with brightness temperature measurements are also assumed known. This method was not used here because of the prohibitive number of calculations required to evaluate $S_{\mathbf{T}, \mathbf{T}_b} S_{\mathbf{T}_b}^{-1}$. In addition, the strict use of correlation tends to obscure the magnitude of the causes of the brightness fluctuations and their relation to profile fluctuations.

The procedure used here directly relates a linear approximation of the brightness equation to the desired profile fluctuations using eq (1), (2), and (3). In addition to reducing the number of brightness calculations to one, namely the brightness of the average profile, this procedure has the advantage of explicitly showing the separate contributions to the variance of the brightness fluctuations by each of the atmospheric parameters.

The monochromatic brightness at an initial elevation angle, θ , is given by

$$T_b(\theta) = \int_0^\infty dh T \alpha \csc \theta e^{-\int_0^h dh' \alpha \csc \theta} \quad (4)$$

where h is height, and the absorption coefficient, α , is a function of temperature, T , pressure, p , and relative humidity, r (Staelin 1969). Because of atmospheric refraction and earth curvature, the local elevation angle along a ray path is a (usually weak) function of height and refractive index profile. By expanding the integrand of eq (4) in a Taylor series about the mean profiles of T , p , and r , and then averaging over their joint distribution, it is seen that, to the second order, the average brightness at a fixed initial elevation is the brightness of the average profile:

$$\langle T_b(\theta) \rangle = \int_0^\infty dh \langle T \rangle \langle \alpha \rangle \langle \csc \theta \rangle e^{-\int_0^h dh' \langle \alpha \rangle \langle \csc \theta \rangle}. \quad (5)$$

In eq (5), the ensemble average of $\csc \theta$ has been indicated because of the dependence of refractive bending on profile variations. The linear terms in the Taylor expansion are

$$\begin{aligned} T'_b(\theta) &\equiv T_b(\theta) - \langle T_b(\theta) \rangle \\ &= \int_0^\infty dh [I_T(\theta, h) T'(h) + I_p(\theta, h) p'(h) + I_r(\theta, h) r'(h)] \end{aligned} \quad (6a)$$

where $T'(h) \equiv T(h) - \langle T(h) \rangle$, etc., and

$$I_T(\theta, h) = \left. \frac{\partial}{\partial T(h)} \left(T \alpha \csc \theta e^{-\int_0^h \alpha \csc \theta dh'} \right) \right|_{\text{mean profile}}, \quad (6b)$$

$$I_p(\theta, h) = \langle T(h) \rangle \left. \frac{\partial}{\partial p(h)} \left(\alpha \csc \theta e^{-\int_0^h \alpha \csc \theta dh'} \right) \right|_{\text{mean profile}}, \quad (6c)$$

and

$$I_r(\theta, h) = \langle T(h) \rangle \left. \frac{\partial}{\partial r(h)} \left(\alpha \csc \theta e^{-\int_0^h \alpha \csc \theta dh'} \right) \right|_{\text{mean profile}}. \quad (6d)$$

The coefficient $I_T(\theta, h)$ reduces to the usual definition of the temperature weighting function, as given, for example, by Meeks and Lilley (1963), when the temperature dependence of the absorption coefficient is neglected. In practice, the above integrals cannot be evaluated analytically and must be reduced to computational form. Introducing a suitable quadrature approximation involv-

ing m points on the profile leads to the matrix equation

$$\mathbf{T}'_b = A_T \mathbf{T}' + A_p \mathbf{p}' + A_r \mathbf{r}' \quad (7)$$

In eq (7), each component of the $n \times 1$ vector \mathbf{T}'_b is the departure of the brightness temperature from its average at the chosen set of discrete elevation angles, each component of the $m \times 1$ vectors \mathbf{T}' , \mathbf{p}' , and \mathbf{r}' is the departure of the profile from its average at each quadrature height, and the i, j element of the $n \times m$ matrix A_T , say, is the derivative of the i th brightness with respect to the temperature at the j th level. The average accuracy of the linear approximation is a function of second and higher order derivatives of the integrand of eq (4) and of the distribution of T , p , and r . To the second order, the mean square error in the linear approximation of a function, $f(x)$, of a random variable, x , is

$$\frac{d^2 f(\langle x \rangle)}{dx^2} \frac{\sigma_x^2}{2}$$

and, hence, will be small if either the variance, σ_x^2 , or the second derivative is small. The accuracy of the approximations used here are evaluated numerically in sections 5 and 6.

Any brightness temperature measurement will be in error by an amount ϵ , where ϵ is a random variable that is uncorrelated with atmospheric fluctuations. These errors will be caused by receiver noise fluctuations, antenna side lobes, lossy wave guides, etc. It is assumed that any bias present in the measurement can be removed experimentally so that ϵ has zero mean. In the linear approximation, we may express the measured brightness, $\mathbf{T}'_b^{(m)}$ (relative to its mean), as the sum of the atmospheric contribution, \mathbf{T}'_b , and an $m \times 1$ error vector ϵ as

$$\mathbf{T}'_b^{(m)} = \mathbf{T}'_b + \epsilon \quad (8)$$

and

$$\mathbf{T}'_b^{(m)} = A_T \mathbf{T}' + A_p \mathbf{p}' + A_r \mathbf{r}' + \epsilon \quad (9)$$

To derive a temperature profile \mathbf{T}' from measurements $\mathbf{T}'_b^{(m)}$ by eq (1) requires the autocovariance matrix of the brightness, $S_{T_b^{(m)}}$ and the cross-covariance matrix between the temperature and the brightness, $S_{T, T_b^{(m)}}$. Under the above assumptions, these matrices may be straightforwardly evaluated using eq (2), (3), and (9) to yield

$$S_{T_b^{(m)}} = A_T S_T A_T^* + A_T S_{T_p} A_p^* + \dots + A_r S_{T_r} A_r^* + A_p S_p A_p^* + S_\epsilon \quad (10)$$

and

$$S_{T, T_b^{(m)}} = S_T A_T^* + S_{T_p} A_p^* + S_{T_r} A_r^* \quad (11)$$

Equation (10) relates the variance in measured atmospheric brightness to the variance at each of the points on the profiles of the temperature, pressure, and humidity and instrumental noise; the matrix $S_{T, T_b^{(m)}}$ expresses the degree of correlation between temperature fluctuations and brightness measurements. The random vectors \mathbf{p}' , \mathbf{r}' , and ϵ may also be estimated by

equations identical in form to eq (9) and (10). Two special cases of the above equations may be noted. First, if A_p and A_r are negligible, that is, if the spectral region or meteorological conditions are such that pressure and water vapor effects are small, then the above equations reduce to those of Rodgers (1966) and Strand and Westwater (1968):

$$S_{T_b^{(m)}} = A_T S_T A_T^* + S_\epsilon, \quad (12)$$

and

$$S_{T, T_b^{(m)}} = S_T A_T^* \quad (13)$$

Second, if the cross-covariance matrices between temperature and the other two atmospheric parameters are negligibly small, then we again get eq (13), but

$$S_{T_b^{(m)}} = A_T S_T A_T^* + S_\epsilon^{(e)} \quad (14)$$

where

$$S_\epsilon^{(e)} = S_\epsilon + A_p S_p A_p^* + A_p S_{pr} A_r^* + A_r S_{rp} A_p^* + A_r S_r A_r \quad (15)$$

This explicitly shows that atmospheric fluctuations that are uncorrelated with temperature fluctuations have the same effect as instrumental noise. It also implies that if the "effective" noise level, $S_\epsilon^{(e)}$, is dominated by background fluctuations of atmospheric origin, then very little improvement in inversion results can be achieved by lowering of instrumental noise levels alone.

The linear eq (6) were expressed with temperature, pressure, and humidity as functions of height. It would also be possible to express the equations in terms of temperature and humidity as a function of pressure by using the hydrostatic equation. For ground-based applications, the greatest difficulty with this approach is the construction of various averages appropriate to the variable surface pressure.

When ground-based remote measurements are made, they can frequently be supplemented with direct measurements of surface values of the parameter(s) to be inferred. For example, surface measurements of temperature, pressure, and relative humidity can easily be taken. The value of the surface temperature can then be used as an exact mathematical constraint on the solution of the integral equation. When statistical inversion methods are used, the laws of conditional probability allow the use of additional statistical constraints that modify the estimate of the function at each point of the profile. These constraints frequently considerably reduce the a priori variance of the temperature profile. In addition, the pressure and humidity constraints reduce the effective noise level, $S_\epsilon^{(e)}$. In particular, since pressure fluctuations tend to be highly correlated over broad height intervals, the pressure constraint considerably reduces the effective noise from this component.

As in the unconstrained case, we may apply eq (1), (2), and (3) to the inversion problem if:

1. We restrict the expected value operator to range over the conditional distribution of given surface parameters, and
2. We transform the original data vector $\mathbf{T}'_b^{(m)}$ to one that has zero mean with respect to the conditional distribution.

Requirement (1) may be imposed, under the assumption of normality, by applying a standard statistical method using conditional probability to modify each of the covariance matrices occurring in eq (10). The rather cumbersome details of this technique are described by Graybill (1961).

An alternate method of incorporating surface measurements is to adjoin the vector of constraints to the vector of brightness measurements to form a "generalized" data vector. Equations (1), (2), and (3) can then be applied directly using the unconstrained distribution.

The transformation of the measured brightness to a quantity that has zero mean with respect to the conditional distribution is achieved by taking the conditional average of eq (9) and subtracting the result from the measured brightness. The mean brightness, conditional upon fixed surface conditions, is related to the ensemble averaged brightness $\langle T_b \rangle$ by

$$\langle T_b | C \rangle = \langle T_b \rangle + A_r (\langle T | C \rangle - \langle T \rangle) + A_p (\langle p | C \rangle - \langle p \rangle) + A_r (\langle r | C \rangle - \langle r \rangle). \quad (16)$$

Above, C refers to the triplet of fixed surface constraints, T_1, p_1 , and r_1 and the notation $\langle V | C \rangle$ designates the conditional average of the vector V , given C . In section 5, results of inversions are given using both constrained and unconstrained statistical methods.

Although we have presented only linear techniques above, the extension of the statistical method to iterative analysis is straightforward. To apply iterative analysis, each component of the temperature, pressure, and humidity profiles is estimated by the appropriate application of eq (1). These estimates are then used to correct the weighting functions at each stage of the iteration process. The necessity of recorrecting the weighting functions by iteration depends on the experimental noise level: if the linearization errors are larger than the noise levels, then iteration can improve solution accuracy. However, it is not clear that a linearized iterative technique is preferable to the general eq (1) since one of the prime motivators of the linearization technique was to avoid excessive computer calculation. If the system of equations is strongly nonlinear, the use of nonlinear noniterative estimation involving higher order moments of the profile distribution is possible (Staelin 1969). As stated by Swerling (1966), linear estimates are optimum (of all estimates, linear or not) if all quantities are multivariate Gaussian and if the measurement fluctuations are linearly related to the profile fluctuations.

3. WEIGHTING FUNCTIONS

The brightness temperature at frequency ν and elevation angle θ is a weighted average of the temperature distribution over some spatial region. For a stratified atmosphere, the weighted height average is determined by the temperature weighting function given by eq (6b). As a typical example of microwave ground-based temperature weighting functions, figure 1 shows monochromatic

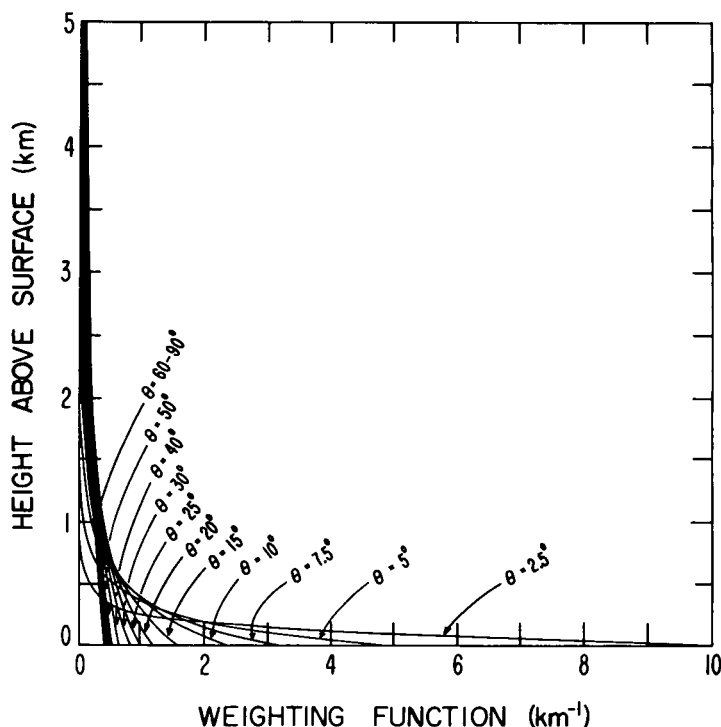


FIGURE 1.—Temperature weighting functions at 54.0 GHz for angular probing. August values are for Salt Lake City, Utah.

weighting functions at 54.0 GHz for discrete elevation angles. These calculations are for the August monthly average profiles of temperature, pressure and relative humidity at Salt Lake City, Utah. The oxygen absorption coefficient is determined using the Van Vleck-Weisskopf (1945) line shape with line width parameters of Carter et al. (1968). The small water vapor contribution was calculated using the same line shape, but with line parameters determined by Westwater (1967). As is evident from the figure, very narrow height resolution is obtained near the surface, but this resolution degrades rapidly with altitude. The corresponding transmission curves for this location and frequency are shown in figure 2.

4. ANALYSIS AND INVERSION OF HAWAIIAN RADIOMETER DATA

The ultimate test of a remote sensing technique is its performance in a field operation. In this and the following section, we derive temperature profiles from microwave radiometer data and compare the results with theoretical predictions and with independent direct temperature measurements. The sequential analysis procedure that we follow is to (1) compare radiometer measurements and brightness calculations to determine effective measurement noise levels; (2) perform theoretical calculations of expected accuracies in inversion results using the noise levels determined in (1); (3) invert the data using the method of section 3; and (4) compare inverted and directly measured profiles.

The Hawaiian data were taken at Upolu Point, Hawaii, Hawaii, during two 2-week periods in April and July-

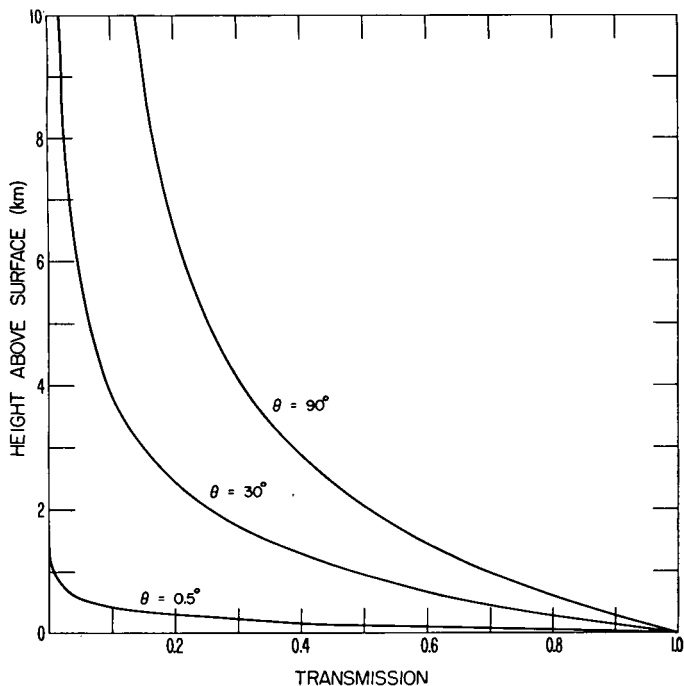


FIGURE 2.—August atmospheric transmission at 54.0 GHz for Salt Lake City, Utah.

August 1968. Thermal emission measurements at 52.5 GHz were made with a microwave radiometer designed and constructed by Jack B. Snider of National Oceanic and Atmospheric Administration (NOAA) Environmental Research Laboratories. Radiosonde observations of temperature, pressure, and relative humidity were taken at 3-hr intervals and covered the height range from the surface to 10 km. Emission measurements at a set of nine fixed elevation angles were taken at 3-hr intervals to coincide with the onsite radiosonde release; the angles were chosen to divide the cosecant into equal increments between the lowest (5.25°) and the highest (90°) elevation angles used.

The data were supplied to the author in the form of antenna temperature versus elevation angle. Before these data could be used for inversion, a study of the bandwidth integration and antenna effects was necessary. The radiometer was a double sideband Dicke type. In this type of receiver, the weak radio frequency signal, ν_{RF} , incident on the antenna is mixed with a strong local-oscillator signal, ν_o , to produce an output power on an intermediate frequency, ν_{IF} . In a double sideband receiver, both the signal frequency $\nu_{RF} = \nu_o + \nu_{IF}$ and the image frequency $\nu'_{RF} = \nu_o - \nu_{IF}$, can be received and amplified at the intermediate frequency ν_{IF} . The predetection bandwidth $\Delta\nu$ is usually determined by the IF amplifier. The effective bandwidth filter function is indicated schematically in the lower left portion of figure 3. To determine the effect of this bandwidth integration on the brightness temperature and on the profile weighting functions defined by eq (6), numerical calculations were performed assuming Gaussian bandwidths and the radiometer parameters given in figure 3. A seven point Gauss-hermite quadrature was used in integrating each side of the band. Integrating

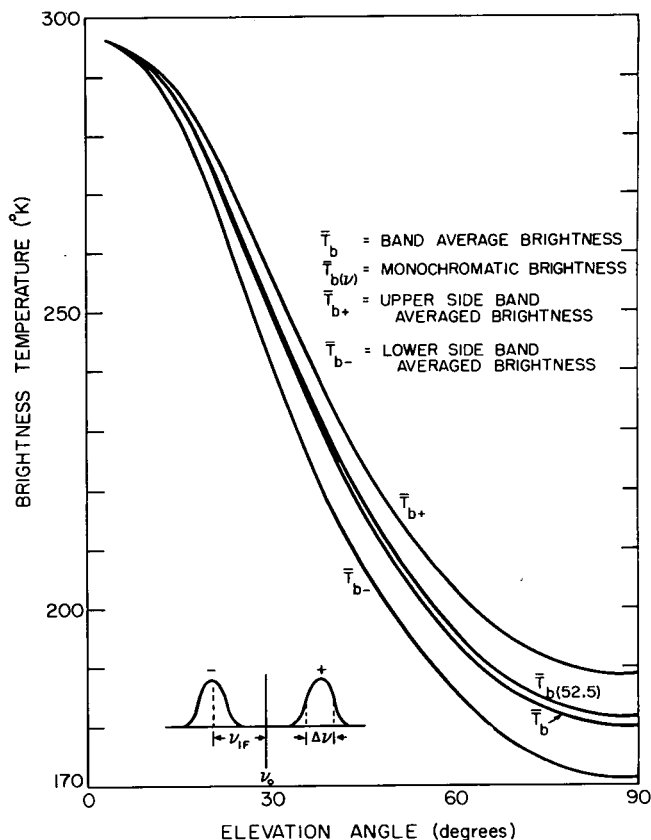


FIGURE 3.—Band averaged brightness for a double side band radiometer for the mean atmosphere at Upolu Point, Hawaii, Hawaii ($\nu_o = 52.5$ GHz, $\nu_{IF} = 160$ MHz, $\Delta\nu = 40$ MHz).

the brightness of the mean Hawaiian atmosphere during the period of observation resulted in a maximum difference of about 1.5°K; the complete results are shown in the figure. To test the sensitivity of these results to profile variations, bandwidth calculations for two extreme profiles were performed; again, the differences between integrated and monochromatic brightness were the same to within about 0.02°K. Thus, for the frequency characteristics of this radiometer, and if departures from the mean brightness are used, we may make the approximation of replacing double sideband averages by the value at the center frequency.

The antenna used in collecting the emission data was a 4-ft Cassegrain-type parabolic dish with a half-power main beam width of about 0.2°. Any antenna measures a weighted brightness distribution over a sphere; for a narrow beam antenna with low side lobes, the antenna and brightness temperature are approximately equal. For the antenna described above, such was not the situation as is evident from figure 4 which shows the average of 84 antenna temperature measurements versus the band average brightness calculated for the average profile during the same period. Included in the average of T_A were some data taken in the presence of clouds. Clouds showed little effect, however, except during periods of rain and heavy overcast, periods which were excluded from the average. The standard method of converting T_A to T_b

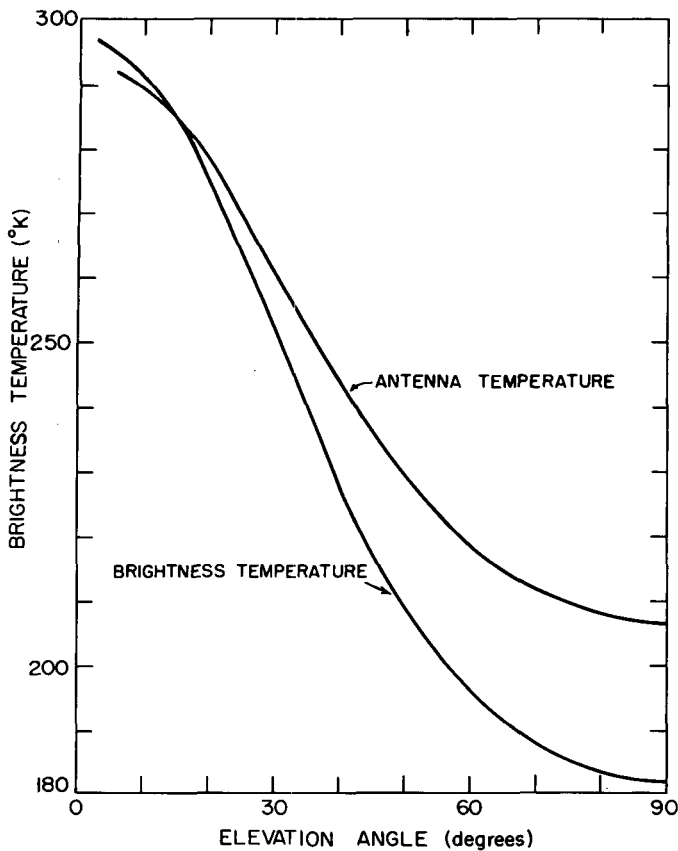


FIGURE 4.—Average antenna and brightness temperature for Upolu Point, Hawaii, Hawaii, July-August 1968 ($\nu=52.5$ GHz).

requires convolution of a known gain pattern with a background brightness model to estimate the stray contribution to T_A from outside the main beam. The stray contribution is then subtracted from T_A to get T_b . For the dish antenna used in Hawaii, the gain pattern was known only for a few degrees surrounding the main beam, and the above method could not be used. A statistical technique of estimating T_b from T_A will be described below. The equation relating the two, namely,

$$T_A(\theta, \varphi) = \frac{1}{4\pi} \int_{\Omega} G(\theta, \varphi; \theta', \varphi') T_b(\theta', \varphi') d\Omega' \quad (17)$$

where θ and φ are elevation and azimuth in polar coordinates, and $d\Omega$ is an element of solid angle, is similar in form to an integral equation of the first kind. If noiseless measurements of $T_A(\theta, \varphi)$ were made for all (θ, φ) and if the antenna gain function, $G(\theta, \varphi; \theta', \varphi')$, were known, then in principle (eq 17) could be inverted to determine $T_b(\theta, \varphi)$, at least for gain functions with good angular resolution. In practice, only a finite number of imperfect measurements are available. However, in a manner similar to the technique used in the statistical inversion of the transfer equation, the antenna temperature measurements may be used as estimators of the desired brightness temperatures; thus

$$\hat{T}_b(\theta) = \sum_i C_i(\theta) T_{A_i} \quad (18)$$

TABLE 1.—Measurement noise level

	Elevation angle (degrees)								
	5.625	11.25	16.875	22.5	28.125	33.75	39.375	45.0	50.625
σ_{T_b} (°K)	0.76	0.76	0.59	0.63	0.76	0.71	0.61	0.82	0.73

where the summation extends over the number of observed antenna temperatures, T_{A_i} . Physically, it is reasonable to assume that T_b could be approximated by a weighted sum of well-chosen antenna temperatures since T_A is a weighted average of T_b . The coefficients, $C_i(\theta)$, could be determined by the least-squares criterion if a simultaneous collection of correct brightness temperatures and corresponding antenna temperatures were available over a representative ensemble of atmospheric (and surface) conditions. In this way, measurements of surface emission could be used to improve estimates of sky brightness. Assuming the correctness of the analytical absorption equations, the "correct" brightness can be approximated by calculations based upon onsite radiosonde observations. The correctness of the absorption equations may be (and were) independently checked by other methods such as comparison of attenuation calculations based on radiosonde observations with zenith attenuation measurements. To apply this technique to the Hawaiian data, 25 radiometer-radiosonde profile pairs were selected at random and excluded from the 84 original data pairs for later use in inversion. The weighting coefficients, $C_i(\theta)$, were determined by least squares over the remaining data. The results of using the $C_i(\theta)$ to predict the original 25 brightness temperatures are shown in table 1. The average standard deviation per angle was 0.72°K . This is about an order of magnitude greater than the theoretical receiver sensitivity, which was 0.13°K for the $2\frac{1}{2}$ -min averaging time.

An important point in the development of the inversion method derived in section 2 is the assumption that brightness fluctuations may be linearly related to profile fluctuations. In the microwave region, where the Planck function is a linear function of temperature, linearity requires fluctuations in the kernel (derivative of the transmissivity) to be linearly related to profile fluctuations. The accuracy of the linear approximation was evaluated exactly at 52.5 GHz for all 25 profiles used in inversion and at 54.5 GHz for two extreme profiles. For the lower frequency, where the emission is strongly affected by water vapor fluctuations, the rms linearization error at zenith elevation was 0.36°K ; the error at $\theta=5.25^\circ$ was 0.07°K . It was also noticed that the zenith linearization error had an average bias of -0.25°K . At 54.5 GHz, where the variance of the weighting function is much less, the maximum linearization errors were less than 0.1°K .

The linear model developed in section 2 can be applied to the determination of the atmospheric contributions to ground-based observations of brightness fluctuations. At low elevation angles, where the radiometer is viewing the optically opaque portion of the atmosphere, intensity

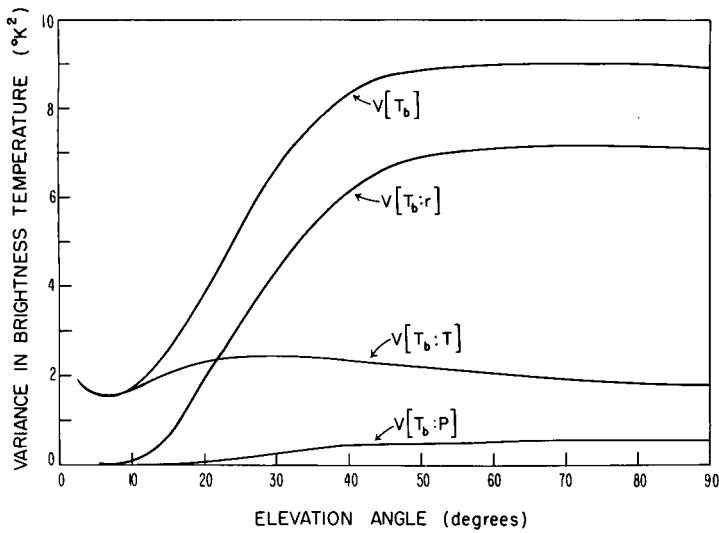


FIGURE 5.—Relative contribution to fluctuations in brightness temperature at Upolu Point, Hawaii, Hawaii, for April and July-August ($\nu=52.5$ GHz, T is temperature, r is relative humidity, p is pressure).

fluctuations are caused primarily by temperature fluctuations; for higher angles, where the optical depth is less, fluctuations in optical depth may add a component to the observed intensity fluctuations. The quantitative description of the relative contributions to the atmospheric brightness fluctuations is

$$S_{T_i} = A_T S_T A_T^* + A_r S_r A_r^* + \dots + A_p S_p A_p^* \quad (19)$$

The diagonal elements of S_{T_i} are the variances of atmospheric brightness at the chosen set of angles; the off-diagonal elements represent the covariances between brightness temperatures at different angles. The brightness variance at the i th angle due to the integrated effect of temperature fluctuations, say, is the i th diagonal element of $A_T S_T A_T^*$. Figure 5 shows the diagonal elements of the various matrices as a function of elevation angle for the April-July-August Hawaiian ensemble. In the notation used here, $V[T_b:T]$ is the contribution to the variance of T_b due to fluctuations in temperature alone; $V[T_b]$ is the total variance of T_b . The correlation effects between the three parameters p , T , and r are small as shown by approximate equality of the sum of the three partial variances and the total variance $V[T_b]$. The surprising feature demonstrated by this figure is the large contribution to the variance at the higher elevation angles by the moisture fluctuations. The water vapor contribution to the average brightness is large because of the large amount of water contained in the narrow height interval from the surface to the base of the trade wind inversion. The water vapor variance is particularly large for this ensemble because of the contrast between the normal trade wind pattern that was present in much of the July-August data and the 2-week period in April when the trade wind pattern was interrupted by the so-called kona winds. For this period, in which the trade

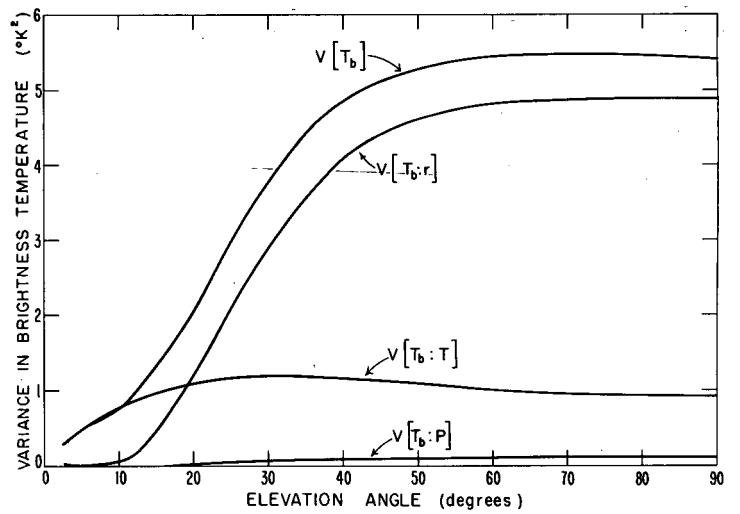


FIGURE 6.—Same as figure 5 except constrained surface conditions.

wind inversion was absent, the water vapor was distributed to much higher altitudes.

As discussed in section 2, atmospheric fluctuations that are uncorrelated with the temperature have the same effect on the inversion process as instrumental noise. Thus, figure 5 shows that for the higher elevation angles, the effective signal to noise ratio is less than unity. The obvious way to reduce this noise level would, of course, be to measure the emission around the 22.235 GHz water vapor line. Because a radiometer at this frequency was not available, only surface constraints were available to reduce the noise level. Figure 6 shows the resulting contributions to the variance in brightness for fixed surface conditions. Since the variance in moisture distribution was primarily related to the presence or absence of the trade wind inversion, the surface constraints do little to affect this component of variance. As is evident from the figures for both constrained and unconstrained distributions, the pressure effect is small. The fractional reduction of the pressure contribution by surface constraints is substantial, here and in general, because pressure distributions tend to be highly correlated. Meteorological conditions where pressure fluctuations can contribute 1 to 2 $(^\circ\text{K})^2$ to the zenith brightness variance are not uncommon.

Statistical techniques can be used to predict the accuracy that can be achieved by inverting indirect measurements (Westwater and Strand 1968). This accuracy is a function of the statistical characteristics of the vertical temperature structure, the shape of the weighting functions, the measurement noise level, and the number of measurements used. The accuracies expected for Hawaiian statistics constrained to surface conditions and experimental noise levels determined for various sets of the 52.5 GHz radiometer data are shown in figure 7. Here, the curve labeled σ_T shows the a priori standard deviation in temperature as a function of height. The residual standard errors of estimate to be expected after inverting measurements with the three noise levels (average per angle for nine angles), are also plotted as a function of height. Thus,

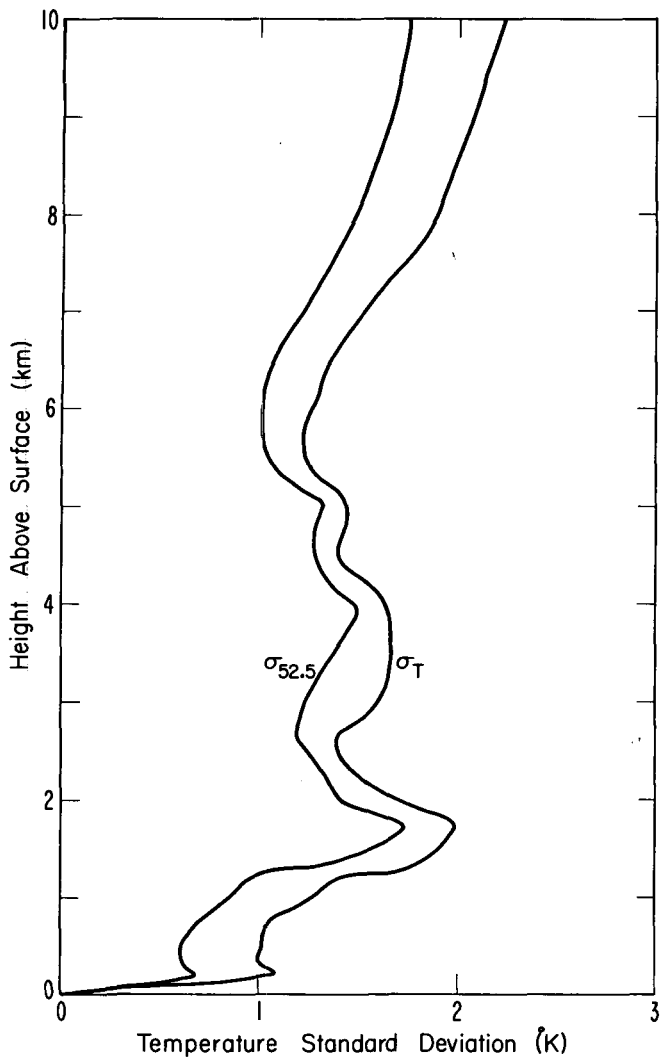


FIGURE 7.—Theoretical resolution in standard deviation of Upolu Point, Hawaii, Hawaii, temperature profiles (constrained to surface conditions) by inversion of 52.5 GHz radiometer data. (Nine angles, $\sigma_\epsilon = 0.72^\circ\text{K}$.)

the average accuracy expected from inversion with measurements of the assumed accuracies is about 1°K rms error. The intersection of the residual error curves occurs because of correlation of angular measurement errors.

The statistical inversions of the previously described 25 sets of angular brightness temperature measurements were performed using both constrained and unconstrained statistics. These profiles were excluded from the statistical ensemble used in constructing the relevant covariance matrices. Figure 8 shows typical inversion results. In both cases, the inverted profile is a smoothed version of the original, with a smoothing that is commensurate with the effective noise levels. Note that the trade wind inversion at 2 km is smoothed out; the average rms deviation per point is around 1°K , a figure not out of line with theoretical predictions. The effect of using constrained methods is shown in figure 9 where constrained and unconstrained inversions are compared for the same profile. Using constrained statistics lowers the effective noise level and

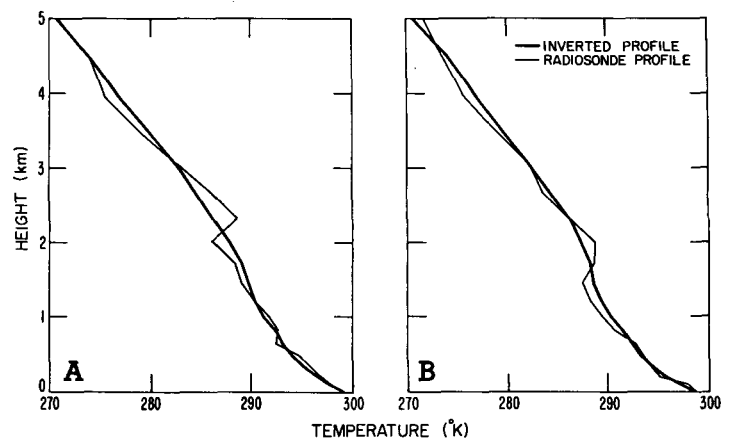


FIGURE 8.—Upolu Point, Hawaii, Hawaii, temperature profile derived from radiometer measurements at 52.5 GHz using constrained statistics for (A) 1700 HST, July 23, and (B) 0003 HST, July 28.

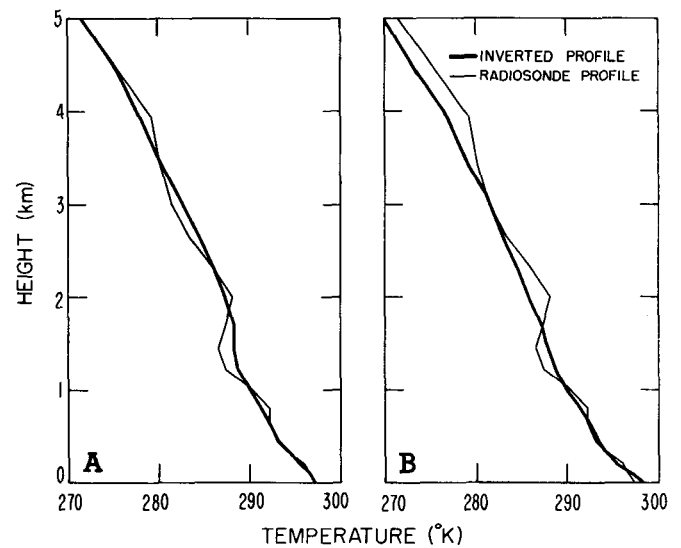


FIGURE 9.—Upolu Point temperature profile derived from radiometer measurements at 52.5 GHz for 0606 HST, July 28, using (A) constrained statistics and (B) unconstrained statistics.

allows some of the higher frequency spacial components to be present in the solution.

The summary of constrained inversion results is shown in table 2. The tabulated quantities represent average rms errors between the inverted profile and the radiosonde profile at each quadrature height. The indicated 90-percent confidence limits were determined using the χ^2 -test with 25 degrees of freedom. The improvement over a priori statistics is evident as shown, with the exception of the 2.00-km level. The statistics there reflect that the trade wind inversion is being smoothed out in the solution. The improvement over the original statistics is not particularly large because (1) their variance is small and further reduction is difficult, (2) the vertical profiles have poor autocorrelation (Westwater 1970), and (3) the contaminating effect of water vapor gives rise to large effective noise levels at the higher elevation angles. The average rms

TABLE 2.—Summary of Hawaiian constrained inversion results ($\nu=52.5$ GHz, 9 angles). Data are based on 25 profiles at 90-percent confidence intervals. T is radiosonde temperature profile, \hat{T} is inverted temperature profile, \bar{T} is constrained mean profile.

Height (km)	$\frac{1}{25} \Sigma (T-\bar{T})^2$	$\frac{1}{25} \Sigma (T-\hat{T})^2$	$\sqrt{\frac{1}{25} \Sigma (T-\bar{T})^2}$	$\sqrt{\frac{1}{25} \Sigma (T-\hat{T})^2}$
	(°K) ²	(°K) ²	(°K)	(°K)
0.000	0.000	0.000	0.000	0.000
0.350	0.52 (0.35, 0.88)	0.37 (0.25, 0.63)	0.72 (0.59, 0.94)	0.61 (0.49, 0.80)
0.648	0.62 (0.41, 1.06)	0.44 (0.29, 0.75)	0.79 (0.64, 1.03)	0.66 (0.54, 1.02)
1.013	2.50 (1.66, 4.27)	2.22 (1.47, 3.80)	1.58 (1.30, 2.10)	1.49 (1.15, 1.46)
1.458	4.01 (2.66, 6.86)	3.28 (2.17, 5.60)	2.00 (1.64, 2.63)	1.81 (1.29, 2.38)
2.001	4.01 (2.66, 6.86)	3.96 (2.63, 6.77)	2.00 (1.64, 2.63)	1.99 (1.63, 2.60)
3.050	1.29 (0.85, 2.21)	0.75 (0.50, 1.28)	1.13 (0.93, 1.50)	0.87 (0.71, 1.14)
3.946	3.41 (2.26, 5.83)	2.72 (1.80, 4.65)	1.85 (1.51, 2.42)	1.65 (1.35, 2.16)
5.040	1.27 (0.84, 2.17)	1.14 (0.76, 1.95)	1.17 (0.92, 1.48)	1.07 (0.88, 1.40)
6.376	1.61 (1.06, 2.75)	1.20 (0.79, 2.05)	1.27 (1.03, 1.67)	1.09 (0.89, 1.44)
8.008	2.40 (1.59, 4.10)	1.67 (1.11, 1.90)	1.55 (1.27, 2.02)	1.29 (1.06, 1.39)
10.000	3.90 (2.59, 6.67)	1.89 (1.25, 3.23)	1.98 (1.62, 2.60)	1.38 (1.13, 1.80)
Average of 25 points to 10 km				
	2.002	1.604	1.414	1.265

TABLE 3.—Comparison of experimental versus theoretical accuracies in inversion ($\nu = 52.5$ GHz, 9 angles). Data are based on 25 profiles at 90-percent confidence intervals. T , \bar{T} , and \hat{T} have the meanings given in table 2.

Height (km)	$\sigma(T-\bar{T})$	$\sqrt{\frac{1}{25} \Sigma (T-\bar{T})^2}$	$\sigma(T-\hat{T})$	$\sqrt{\frac{1}{25} \Sigma (T-\hat{T})^2}$
	(°K)	(°K)	(°K)	(°K)
0.000	0.000	0.000	0.000	0.000
0.350	0.99	0.72 (0.59, 0.94)	0.61	0.61 (0.49, 0.80)
0.648	1.04	0.79 (0.64, 1.03)	0.66	0.66 (0.54, 1.02)
1.013	1.30	1.58 (1.30, 2.10)	0.89	1.49 (1.15, 1.46)
1.458	1.89	2.00 (1.64, 2.63)	1.54	1.81 (1.21, 2.38)
2.001	1.68	2.00 (1.64, 2.63)	1.40	1.99 (1.63, 2.60)
3.050	1.64	1.13 (0.93, 1.50)	1.24	0.87 (0.71, 1.14)
3.946	1.64	1.85 (1.51, 2.42)	1.50	1.65 (1.35, 2.16)
5.040	1.44	1.17 (0.92, 1.48)	1.33	1.07 (0.88, 1.40)
6.376	1.34	1.27 (1.03, 1.67)	1.05	1.09 (0.89, 1.44)
8.008	1.90	1.55 (1.27, 2.02)	1.50	1.29 (1.06, 1.39)
10.000	2.19	1.98 (1.62, 2.60)	1.76	1.38 (1.13, 1.80)
Average of 25 points to 10 km				
	1.49	1.42	1.20	1.27

accuracy to 10 km is 1.27°K as compared with an accuracy of 1.42°K achieved by using only constrained statistics.

As mentioned above, the theory of statistical estimation allows prediction of the accuracies to be achieved by inversion. In table 3, a comparison of theoretical predictions versus experimental results are shown. The theoretical values represent square roots of the diagonal elements of the appropriate covariance matrices; the solution covariance matrix was calculated using the effective noise level, $S_e^{(e)}$ given by eq (15), a procedure that neglects the correlation effects between temperature and the other variables. As is evident from inspection, the numbers usually agree within the 90-percent confidence limits.

The inversion equations developed in section 2 can be used to estimate each component contributing to the measured brightness fluctuations. This includes, in addition to temperature, the pressure, relative humidity, and experimental error components. The 25 measurements described above, when inverted for pressure and relative humidity profiles, allowed a reduction in average rms error per point (constrained surface conditions) from 0.78 to 0.62 mb in pressure and 1.57 to 1.35 gm⁻³ in absolute humidity. The absolute humidity inversions were achieved by linearly inverting the temperature and relative humidity profiles and then combining these to form the absolute humidity. In addition to profile estimation, the

point estimates of absolute humidity were integrated with respect to height to form estimates of the total vertical water content. The water content, as determined by numerically integrating the 25 radiosonde soundings, averaged $2.85 \text{ g}\cdot\text{cm}^{-2}$ with a range of $1.95\text{--}4.18 \text{ g}\cdot\text{cm}^{-2}$. The rms deviation between radiometrically inferred and radiosonde measured water content was $0.21 \text{ g}\cdot\text{cm}^{-2}$ and corresponded to a correlation coefficient of 0.92. This was an improvement over constrained statistics by about 6 to 1.

5. ANALYSIS AND INVERSION OF SALT LAKE CITY RADIOMETER DATA

The application of microwave radiometry to remote probing of low altitude temperature profiles is being investigated experimentally by Sperry Rand Corporation (Mount et al. 1968). To further test statistical inversion techniques on microwave data, we procured data from one of their field tests. The analysis and inversion of these data are discussed in this section.

The data were taken at Salt Lake City, Utah, on Aug. 15 and 16, 1968, during clear daytime conditions. Null balance radiometer measurements of thermal emission at discrete elevation angles ranging from horizontal to zenith were taken at 54.0, 54.5, and 55.0 GHz. The radiometer measurements had been reduced to brightness temperature by Sperry Rand and were supplied to the author in this form. Supplementing the radiometer data were onsite radiosonde soundings of height, pressure and temperature extending to 400 mb or approximately 6 km above the surface; the meteorological package did not have a humidity sensor. Nine radiometer runs and six balloon soundings were taken.

As will be seen, for the 54–55 GHz frequency interval, theoretical calculations show that detailed information about the temperature structure above 3 or 4 km would be difficult to obtain by inversion of radiometer data. Nevertheless, at high elevation angles the radiometer can detect gross changes in atmospheric structure above 6 km. Calculations of vertical brightness using the Salt Lake City mean atmosphere indicated that a $10^{\circ}\text{--}30^{\circ}\text{K}$ contribution would arrive at the ground from the thermal emission above 6 km (the transmissivity from 0 to 6 km was 0.23 at 54 GHz). Since meteorological coordinates were not available above 6 km from the onsite soundings, the August mean profiles of temperature, pressure, and humidity were used above the termination point for the brightness calculations described below. Changing the upper level profile from the Salt Lake City August mean to a standard atmosphere resulted in a 3°K change at 54 GHz, a 0.5°K change at 54.5 GHz, and a negligible change at 55 GHz, so that at least one of the channels was sensitive to gross changes in the atmosphere above 400 mb.

The humidity up to 6 km was estimated from the radiosonde observations at the Salt Lake City airport, roughly one mile away from the radiometer field site. At the surface, the absolute humidity was about 4 gm^{-3} . Calculations of wet and dry absorption indicated that the relative

water vapor contribution was small at these frequencies. This contrast to the absorption at 52.5 GHz at Hawaii occurs because (1) the water content of Salt Lake City was nearly a factor of three less, and (2) the dry absorption was from three to five times greater, depending on the frequency.

Before attempting to recover temperature profiles from the radiometer data described above, comparisons of measured brightness with brightness calculations based on radiosondes were made. The oxygen line shape parameters of Carter et al. (1968) can be used with confidence here since they were derived from measurements at frequencies almost coincident with the 54.0-, 54.5-, and 55.0-GHz channels. Initial calculations showed an almost constant difference of about 5°K between measurements and calculations of angular brightness. A bias correction, approximately equal to the difference between the ambient surface temperature and the horizontal brightness, removed the major portion of this error. Theoretically, at the highly absorbing frequencies used here, the horizontal brightness is nearly equal to ambient temperature so the magnitude of the correction was reasonable. Using 12 pieces of data at 54 GHz, 18 at 54.5 GHz, and 48 at 55 GHz, a single bias correction was determined for each frequency by least-squares comparison of calculated versus measured brightness. The resulting standard deviations between measured and calculated brightness were 1.47° , 1.28° , and 0.58°K at 54.0, 54.5, and 55.0 GHz, respectively. When the same procedure was applied to half of the above data sample, neither the bias corrections nor the standard deviations changed appreciably from the above values. The results of the calculations and measurements are shown in figure 10. The calculated average brightness temperatures at the corresponding frequency are shown in each graph for comparison and, in addition, the mean brightness calculations are shown separately in figure 11. There is reasonable agreement between measurements and calculations for all of the nine profiles. Note that the largest deviation at $\nu=54.0$ GHz, radiometer time 2000–2020 MDT, August 16 (0200–0220 GMT, August 17), and radiosonde time 1747 MDT (2347 GMT), August 16, occurs when there is about a 2-hr time interval between radiometer and radiosonde observations.

The absence of the bandwidth correction in the above calculations should be noted. The radiometer was a double sideband type with an intermediate frequency of 157.5 MHz and an equivalent rectangular bandwidth of 160 MHz. The filter function was unknown, but calculations assuming a rectangular filter indicated a maximum deviation from linearity of about 1°K at 54 GHz and a negligible effect at 55 GHz. As indicated previously, when departures from averages are considered, the dependence on bandwidth is considerably reduced. The bandwidth effect becomes much more important at lower pressures where resonant line structure is resolved.

The theoretical variance in brightness temperature as a function of elevation angle at each of the three operating

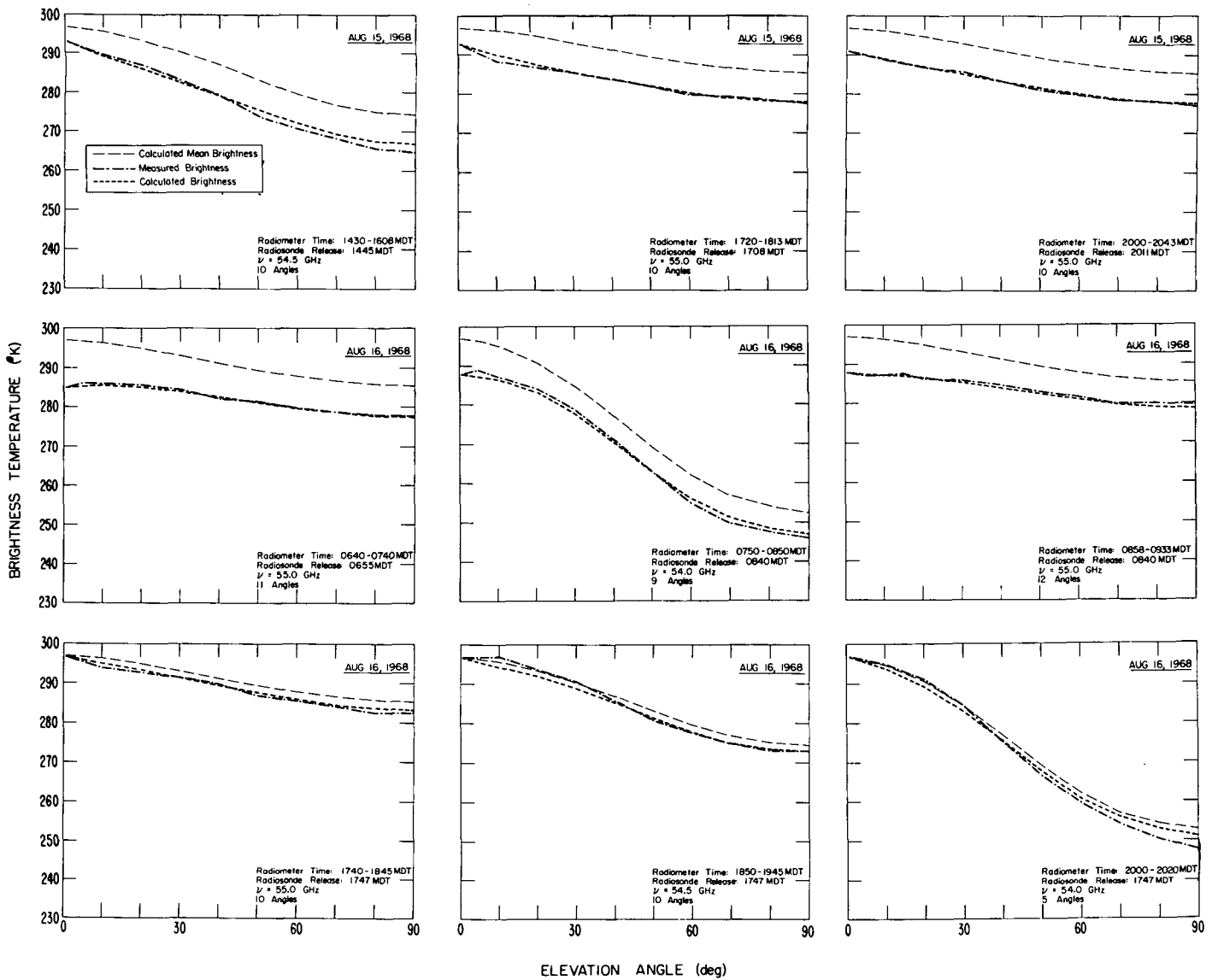


FIGURE 10.—Comparison of measured and calculated brightness temperatures at Salt Lake City, Utah.

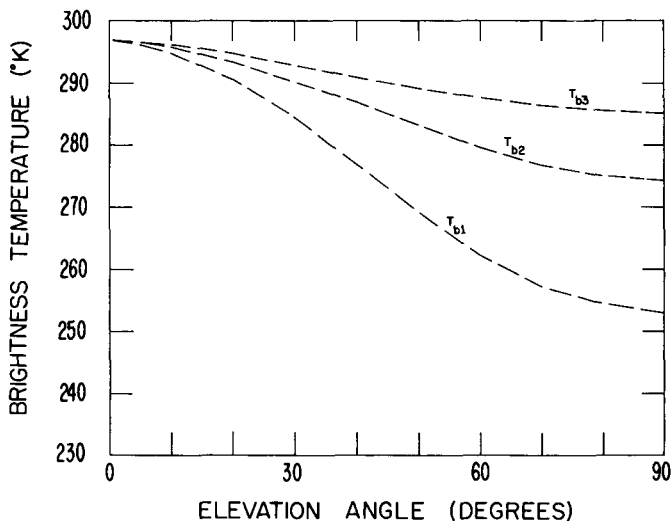


FIGURE 11.—Calculated brightness temperatures at Salt Lake City, Utah ($T_{b1} = 54.0$ GHz, $T_{b2} = 54.5$ GHz, $T_{b3} = 55.0$ GHz).

frequencies was calculated for the Salt Lake City August statistics. The relevant covariance matrices were calculated from a carefully edited ensemble of 5 yr of twice per day radiosonde soundings (287 profiles). In contrast to the variance calculations at 52.5 GHz for Hawaiian climatology, the humidity and pressure fluctuations yielded a contribution to total variance that was 100 to 1 less than that due to temperature fluctuations. The results are shown in figures 12 and 13 for unconstrained and constrained surface conditions, respectively. Note the large variance in the unconstrained case at low elevation angles, reflecting the large dependence on the highly variable surface temperature. Although the imposition of surface constraints considerably lowers the total variance, the resulting signal-to-noise ratio (of variances) is around 25 to 1 for a noise level of 0.5° K.

Following the method described above, the accuracies to be expected from inverting angular measurements at 54.0,

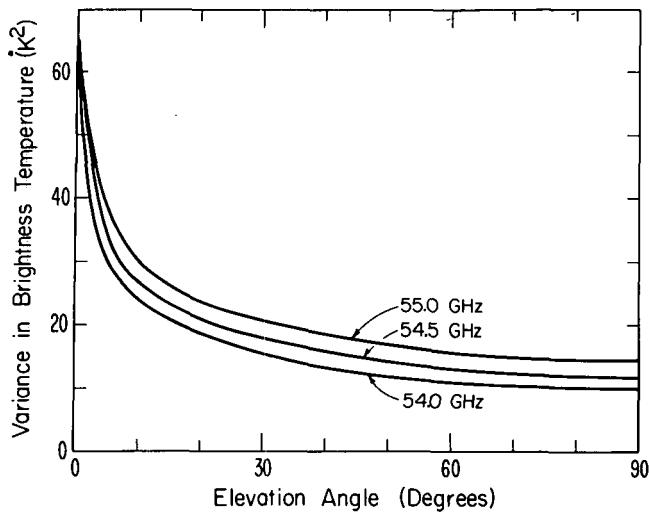


FIGURE 12.—Calculated unconstrained variance in brightness temperature at Salt Lake City, Utah, in August.

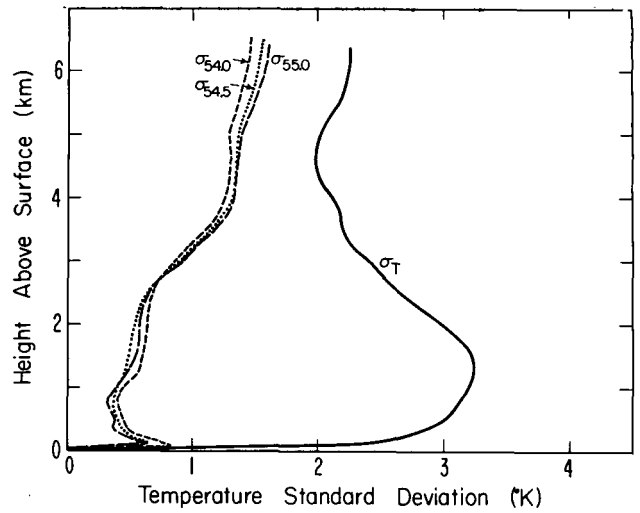


FIGURE 14.—Theoretical reduction in standard deviation of temperature profiles by inversion of microwave radiometer data at Salt Lake City, Utah, in August, using constrained statistics [$\sigma(54.0 \text{ GHz})$, 5 angles, $\sigma_e=1.5^\circ\text{K}$; $\sigma(54.5 \text{ GHz})$, 10 angles, $\sigma_e=1.3^\circ\text{K}$; $\sigma(55.0 \text{ GHz})$, 10 angles, $\sigma_e=0.6^\circ\text{K}$].

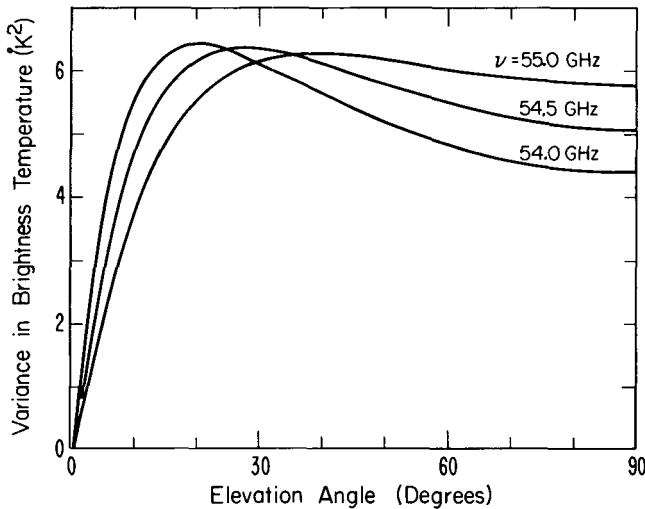


FIGURE 13.—Calculated variance in brightness temperature for constrained surface conditions at Salt Lake City, Utah, in August.

54.5, and 55.0 GHz were calculated. The results, as determined using the Salt Lake City August temperature covariance matrix appropriate to given surface conditions and the effective noise levels determined by comparing measured and calculated brightness, are shown in figure 14. As expected, both the magnitude and the height distribution of the temperature variance are radically different from the Hawaiian ensemble shown previously. A substantial reduction in variance is predicted below 3 km but expected results approach the statistics above this height.

The mathematical inversions of the data described above were achieved by the same techniques that were applied to the Hawaiian ensemble. Pressure and humidity covariance matrices were used in the inversion although

their effect was small. All results shown in figure 15 used covariance matrices appropriate to constrained surface conditions, although strictly speaking the statistics were non-Gaussian (Westwater 1970). Several features of the figures should be noted. First, all inversions of lapse profiles are almost coincident with the radiosonde profiles. This is not simply reproducing the mean, because several of the conditional averages show ground-based thermal inversions. However, when ground-based thermal inversions occur their features are clearly defined. The structure of the elevated isothermal layer occurring at 1445 MDT (2045 GMT) on August 15 is smoothed out. The 3°K maximum difference on the $\nu=55.0\text{-GHz}$ inversion on the August 16, 0840 MDT (1440 GMT) sounding occurs around 4.0 km, well out of the range of this strongly absorbing channel. This is slightly above two standard deviations of the theoretical predictions given previously. Note that the preceding radiometer run at 54.0 GHz at 0750–0850 MDT (1350–1450 GMT), for the same temperature profile, corrects the above errors which suggests that, even with an angular scheme, multispectral measurements can complement each other. These two adjacent radiometer runs also show consistency in indicating a surface-based isothermal layer that the radiosonde does not show. This could result from antenna side lobe effects or from smoothing due to inadequate height resolution.

The inversion results are summarized in table 4. Here, the rms differences between the inverted and the radiosonde profiles are given at selected heights. In addition, the rms differences between the radiosonde soundings and the mean profile, adjusted to the same surface conditions, are shown, so that an indication of the amount of improvement over past statistics can be seen by inspection. Except

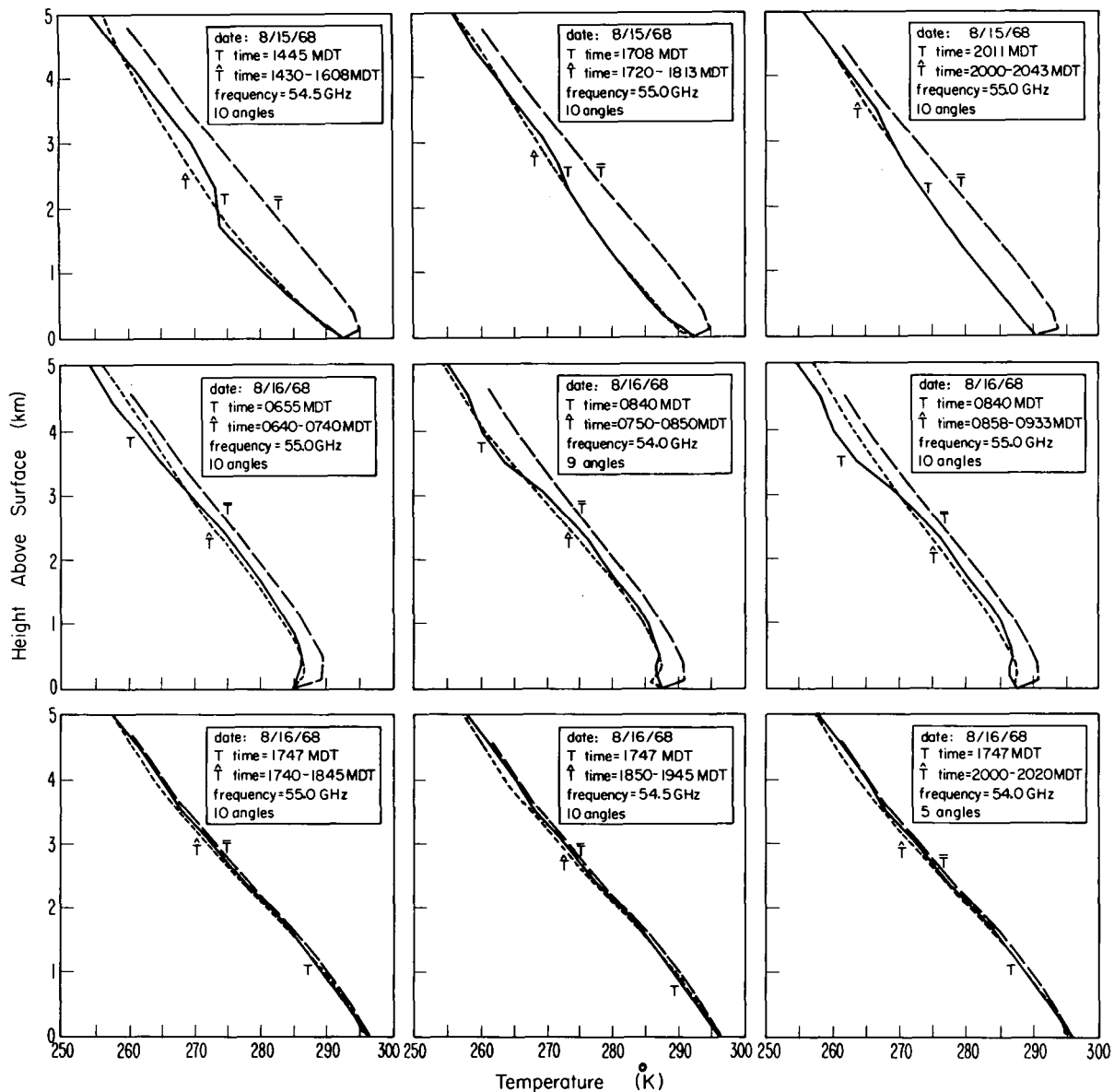


FIGURE 15.—Comparison of inverted and radiosonde temperature profiles at Salt Lake City, Utah. \bar{T} is the constrained mean temperature T is the radiosonde measured profile, \hat{T} is the radiometrically determined profile.

for the 0.105-km level, these inversions give substantial improvement over pure statistics below 3 km. The average improvement in variance was about 25 to 1 over this height interval. As indicated in figure 14, this improvement is expected to diminish rapidly above 3 km for all channels. The resulting rms errors for all three channels show excellent agreement with theory. Note, however, that the numbers represent rms differences and are not errors in inversion unless the radiosonde measures the "true" profile exactly.

6. SUMMARY AND CONCLUSIONS

The technique described here shows promise as a tool for determining low altitude temperature profiles. Microwave angular emission measurements taken at two loca-

tions (during cloudless conditions) were used to recover low altitude profiles with a rms accuracy of about 1°K. Lapse rate and ground-based inversion profiles were successfully inferred, but the details of the Hawaiian trade wind inversion were smoothed out. The accuracies of the inferred profiles agree well with predictions based on the theory of statistical estimation.

Further experimental and theoretical work is necessary to determine the limitations and extension of this technique, particularly in the presence of clouds. Additional refinements in equipment include the use of an antenna with better angular resolution and a radiometer with a multifrequency capacity. A four-channel radiometer developed by the Wave Propagation Laboratory of NOAA will soon be in operation.

TABLE 4.—Comparison of inverted and radiosonde temperature profiles, Salt Lake City, Utah, Aug. 15 and 16, 1968. T , \hat{T} , and \bar{T} have the meanings given in table 2.

Height (km)	$\nu=54.0$ GHz $\sigma_s=1.5^\circ\text{K}$ 2 profiles		$\nu=54.5$ GHz $\sigma_s=1.3^\circ\text{K}$ 2 profiles		$\nu=55.0$ GHz $\sigma_s=0.6^\circ\text{K}$ 5 profiles	
	$\sigma(\bar{T}-T)$	$\sigma(\hat{T}-T)$	$\sigma(\bar{T}-T)$	$\sigma(\hat{T}-T)$	$\sigma(\bar{T}-T)$	$\sigma(\hat{T}-T)$
	(°K)	(°K)	(°K)	(°K)	(°K)	(°K)
0. 00	0. 00	0. 00	0. 00	0. 00	0. 00	0. 00
0. 105	0. 71	0. 93	1. 16	0. 37	0. 92	0. 47
0. 221	1. 07	0. 37	1. 99	0. 35	1. 70	0. 82
0. 350	1. 11	0. 69	2. 76	0. 32	2. 38	0. 50
0. 491	1. 48	0. 21	3. 39	0. 26	2. 72	0. 22
1. 013	2. 75	0. 60	4. 51	0. 59	3. 60	0. 68
1. 458	2. 98	0. 48	4. 96	0. 86	3. 82	0. 65
2. 001	3. 24	0. 66	3. 71	0. 37	3. 93	0. 70
2. 665	3. 46	1. 08	1. 64	1. 67	3. 58	0. 62
3. 050	3. 06	0. 89	1. 55	1. 93	3. 24	0. 66
3. 946	1. 78	1. 08	1. 54	1. 37	2. 69	1. 62
5. 040	2. 98	0. 50	1. 87	1. 48	3. 11	1. 39
Average of 20 points to 6.4 km						
	2. 71	0. 83	3. 16	1. 21	3. 24	0. 88

ACKNOWLEDGMENTS

The author thanks J. London and M. Mizushima of the University of Colorado for many stimulating discussions of this work. Martin T. Decker offered many worthwhile suggestions on the manuscript. The research was supported in part by the Air Pollution Control Office of the Environmental Protection Agency.

REFERENCES

Carter, C. J., Mitchell, R. L., and Reber, E. E., "Oxygen Absorption Measurements in the Lower Atmosphere," *Journal of Geophysical Research*, Vol. 73, No. 10, May 15, 1968, pp. 3113-3120.
 Chahine, Moustafa T., "Inverse Problems in Radiative Transfer: Determination of Atmospheric Parameters," *Journal of the Atmospheric Sciences*, Vol. 27, No. 6, Sept. 1970, pp. 960-967.
 Deutsch, R., *Estimation Theory*, Prentice-Hall Publishing Co., Inc., Englewood Cliffs, N.J., 1965, 269 pp. (see p. 59).
 Foster, Manus, "An application of the Wiener-Kolmogorof Smoothing Theory to Matrix Inversion," *Journal of the Society for Industrial and Applied Mathematics*, Vol. 9, No. 3, Philadelphia, Pa., Sept. 1961, pp. 387-392.

Graybill, Franklin A., *An Introduction to Linear Statistical Models*, Vol. I, McGraw-Hill Series in Probability and Statistics, McGraw-Hill Book Co., Inc., New York, N.Y., 1961, 463 pp. (see pp. 62-63).
 Meeks, M. L. and Lilley, A. E., "The Microwave Spectrum of Oxygen in the Earth's Atmosphere," *Journal of Geophysical Research*, Vol. 68, No. 6, Mar. 15, 1963, pp. 1683-1703.
 Mount, W. D., Anway, A. C., Wick, C. V., and Maloy, C. M., "Capabilities of Millimeter Wave Radiometers for Remotely Measuring Temperature Profiles Pertinent to Air Pollution," *Final Report*, Contract No. PH 86-67-76, Sperry Rand Research Center, Sudbury, Mass., Feb. 1968, 53 pp.
 Rodgers, C. D., "Satellite Infrared Radiometer—A Discussion of Inversion Results," *Memorandum No. 66.13*, Clarendon Laboratory, Oxford University, England, Sept. 1966, 31 pp.
 Smith, W. L., Woolf, H. M., and Jacob, W. J., "A Regression Method for Obtaining Real-Time Temperature and Geopotential Height Profiles From Satellite Spectrometer Measurements and Its Application to Nimbus 3 'SIRS' Observations," *Monthly Weather Review*, Vol. 98, No. 8, Aug. 1970, pp. 582-603.
 Staelin, D. H., "Passive Remote Sensing at Microwave Wavelengths," *Proceedings of the IEEE*, Vol. 57, No. 4, Apr. 1969, pp. 427-439.
 Strand, Otto Neall, and Westwater, Ed R., "Minimum RMS Estimation of the Numerical Solution of a Fredholm Integral Equation of the First Kind," *SIAM Journal of Numerical Analysis*, Vol. 5, No. 2, Society for Industrial and Applied Mathematics, Philadelphia, Pa., June 1968, pp. 287-295.
 Swerling, P., "Topics in Generalized Least Squares Signal Estimation," *Journal of the Society for Industrial and Applied Mathematics*, Vol. 14, No. 5, Philadelphia, Pa., Sept. 1966, pp. 998-1031.
 Van Vleck, J. H., and Weisskopf, V. F., "On the Shape of Collision Broadened Lines," *Reviews of Modern Physics*, Vol. 17, No. 2-3, American Institute of Physics, Inc. New York, N.Y., Apr.-July 1945, p. 227.
 Wark, D. Q., "SIRS: An Experiment to Measure the Free Air Temperature From a Satellite," *Applied Optics*, Vol. 9, No. 8, Aug. 1970, pp. 1761-1766.
 Westwater, Ed R., "An Analysis of the Correction of Range Errors Due to Atmospheric Refraction by Microwave Radiometric Techniques," *ESSA Technical Report IER 30-ITSA 30*, Institute for Telecommunication Sciences and Aeronomy, Boulder, Colo., Mar. 1967, 69 pp.
 Westwater, Ed R., "Ground-Based Determination of Temperature Profiles by Microwaves," Ph. D. thesis, University of Colorado, Boulder, Sept. 1970, 121 pp.
 Westwater, Ed R., and Strand, Otto Neall, "Statistical Information Content of Radiation Measurements Used in Indirect Sensing," *Journal of the Atmospheric Sciences*, Vol. 25, No. 5, Sept. 1968, pp. 750-758.
 Wiener, N., *Extrapolation, Interpolation, and Smoothing of Stationary Time Series*, John Wiley & Sons, Inc., New York, N.Y., 1949, 163 pp. (see chapter II).

[Received April 5, 1971; revised July 6, 1971]